Crystal structure and synchrotron X-ray powder reference pattern for the porous pillared cyanonickelate, Ni(3-amino-4,4′-bipyridine)[Ni(CN)$_4$]

W. Wong-Ng [1,a)] J. Culp,[2,3] J.A. Kaduk [4,5] Y.S. Chen,[6] and S. Lapidus[7]
[1]*Material Measurement Laboratory, National Institute of Standards and Technology, Gaithersburg, MD 20899, USA*
[2]*United States Department of Energy, National Energy Technology Laboratory (NETL), P.O. Box 10940, Pittsburgh, PA 15236-0940, USA*
[3]*United States Department of Energy, NETL Support Contractor, P.O. Box 10940, Pittsburgh, PA 15236-0940, USA*
[4]*Illinois Institute of Technology, Chicago, IL 60616, USA*
[5]*North Central College, Naperville, IL 64540, USA*
[6]*ChemMatCARS, University of Chicago, Argonne, IL 60439, USA*
[7]*Advanced Photon Source, Argonne National Laboratory, Argonne, IL 60439, USA*

(Received 17 July 2023; accepted 15 January 2024)

The structure of Ni(3-amino-4,4′-bipyridine)[Ni(CN)$_4$] (or known as Ni-BpyNH$_2$) in powder form was determined using synchrotron X-ray diffraction and refined using the Rietveld refinement technique (R = 8.8%). The orthorhombic (C*mca*) cell parameters were determined to be a = 14.7218(3) Å, b = 22.6615(3) Å, c = 12.3833(3) Å, V = 4131.29(9) Å^3, and Z = 8. Ni-BpyNH$_2$ forms a 3-D network, with a 2-D Ni(CN)$_4$ net connecting to each other via the BpyNH$_2$ ligands. There are two independent Ni sites on the net. The 2-D nets are connected to each other via the bonding of the pyridine "N" atom to Ni2. The Ni2 site is of six-fold coordination to N with relatively long Ni2–N distances (average of 2.118 Å) as compared to the four-fold coordinated Ni1–C distances (average of 1.850 Å). The Ni(CN)$_4$ net is arranged in a wave-like fashion. The functional group, –NH$_2$, is disordered and was found to be in the *m*-position relative to the N atom of the pyridine ring. Instead of having a unique position, N has ¼ site occupancy in each of the four *m*-positions. The powder reference diffraction pattern for Ni-BpyNH$_2$ was prepared and submitted to the Powder Diffraction File (PDF) at the International Centre of Diffraction Data (ICDD).
© *The Author(s), 2024. Published by Cambridge University Press on behalf of International Centre for Diffraction Data.*
[doi:10.1017/S0885715624000058]

Keywords: Ni(3-amino-4,4′-bipyridine)[Ni(CN)$_4$]), metal-organic framework (MOF), synchrotron powder X-ray studies, disordered Ni-Bpy-NH$_2$ crystal structure

I. INTRODUCTION

The continual rise in anthropogenic CO_2 concentration since the dawn of the industrial revolution and its effect on climate change underlie the urgent need for the implementation of carbon mitigation approaches to stabilize the CO_2 concentration in the atmosphere (Gammon et al., 1985; Etheridge et al., 1996). In the past decades, a great number of possible solid sorbents have been reported throughout the literature. For example, a vast number of metal organic framework (MOF) or coordination polymer compounds that show diverse properties and applications at different pressure and temperature have been developed (Espinal et al., 2009, 2012; Kauffman et al., 2011; Liu et al., 2012; Wong-Ng et al., 2012, 2013, 2015; Furukawa et al., 2013; Gao et al., 2014; Brown and Long, 2014; Queen et al., 2014; Zhou and Kitagawa, 2014; Freund et al., 2021; Unnikrishnan et al., 2021).

The pillared layer is a commonly used motif to build porous coordination polymers or MOFs. Materials based on the pillared cyano-bridged architecture, [Ni'(L)Ni(CN)$_4$]$_n$ (L = pillar organic ligands), or known as PICNICs, have been shown to be diverse where pore size and pore functionality can be varied by the choice of pillar organic ligands. Knowing the orientation of these functional groups in the pore structure is important for correlating their effects on guest adsorption. In addition, a number of PICNICs have been discovered which show reversible structural transitions between low-porosity and high-porosity phases during the adsorption and desorption process of guests. Structural flexibility in PICNICs can be affected by relatively minor differences in ligand design. The physical driving force for variations in host–guest behavior in these materials is still not totally known. One key to understanding this diversity is a detailed investigation of their crystal structures.

Cyano-bridged complexes have been shown to form polymeric structures with 3-D Hofmann-like microporous frameworks (Hofmann and Kuspert, 1897), formed by metal–metal or metal–ligand–metal bridge connections in one, two, or three dimensions. National Energy and Technology Laboratory (NETL) has been one of the leading laboratories in the research area of novel Ni(CN)$_4$-based flexible MOFs (Culp et al., 2008a, 2008b, 2013; Kauffman et al., 2011; Wong-Ng et al., 2013). The precursors of these flexible

[a)]Author to whom correspondence should be addressed. Electronic mail: winnie.wong-ng@nist.gov

https://doi.org/10.1017/S0885715624000058 Published online by Cambridge University Press

TABLE I. Lattice parameters of Ni-BpyNH$_2$ with and without the solvent of crystallization DMSO

	a (Å)	b (Å)	c (Å)	V (Å^3)	Z	D_x (g cm^{-3})
Ni-BpyNH$_2$(D)	14.7000(5)	22.6879(7)	13.8028(4)	4603.4(2)	8	1.570
Ni-BpyNH$_2$	14.7218(3)	22.6615(3)	12.3833(3)	4131.29(9)	8	1.253

Both are orthorhombic with space group *Cmca*. Values inside the brackets are one standard deviation.

MOFs are typically a cyanometallate complex that acts as a ligand and a transition metal complex with available coordination sites. They are collectively called pillared cyanonickelates, or PICNICs. The size of the pores of the materials can be modified by the lengths of the pillared ligands. We have reported a number of PICNIC compounds previously (Wong-Ng et al., 2013, 2016a, 2016b, 2018, 2021a, 2021b; Allen et al., 2015, 2019, 2023; Wong-Ng, 2018; Lawson et al., 2019; Cockayne et al., 2021).

A member of the PICNIC family, namely, Ni (3-amino-4,4′-bipyridine)[Ni(CN)$_4$], or Ni-BpyNH$_2$(D) has been studied previously using single-crystal diffraction method at the microdiffraction facility of the Advanced Photon Source (APS) of the Argonne National Laboratory. The structure of the single crystal was determined to be orthorhombic *Cmca*, $a = 14.7000(5)$ Å, $b = 22.6879(7)$ Å, $c = 13.8028(4)$ Å, $V = 4603.4(2)$ Å^3, and $Z = 8$ (Table I). Highly disordered solvent of crystallization, dimethyl sulfoxide (DMSO) molecules, were located inside the pores. As a result, the chemical formula, $C_{18}Ni_2S_2O_2N_7H_{21}$, is designated as Ni-BpyNH$_2$(D), where D stands for DMSO (Wong-Ng et al., 2016a). Ni-BpyNH$_2$(D) forms a 3-D network, with a 2-D Ni(CN)$_4$ square net connecting to each other via the BpyNH$_2$ ligands.

This paper describes the structure and provides a reference X-ray (synchrotron) powder pattern for the Ni(3-amino-4,4′-bipyridine)[Ni(CN)$_4$], or Ni-BpyNH$_2$ in the powder form. A brief comparison of the structure of Ni-BpyNH$_2$ with Ni-BpyNH$_2$(D) will also be reported. As X-ray powder reference patterns are critical for material analysis, the diffraction pattern for Ni-BpyNH$_2$ has been submitted to the Powder Diffraction File (PDF) of the International Centre for Diffraction Data (ICDD) (Gates-Rector and Blanton, 2019).

II. EXPERIMENTAL

A. Synthesis

We have adopted (with modifications) a procedure originally used by Černák et al. to prepare crystalline 1-D [Ni(CN)$_4$] containing chain compounds (Černák and Abboud, 2000; Wong-Ng et al., 2013, 2016a) for the crystallization of Ni(L)[Ni(CN)$_4$]. The approach involves the use of NH$_3$ as a blocking agent. When a reaction mixture (0.60 mmol of BpyNH$_2$ with 0.5 mmol Ni$_2$(CN)$_4$ hydrate in a mixture of 6 ml H$_2$O, 6 ml concentrated aqueous NH$_3$, and 18 ml DMSO) is warmed in an open flask, the NH$_3$ will outgas from the solution. Using an H$_2$O/DMSO mixture as the solvent and a reaction temperature of ≈90 °C provided the necessary combination of NH$_3$ out gassing rate and oligomer solubility to produce the targeted 3-D polymeric structure. A good crop of crystals can typically be obtained in 24–48 h. The technique has been found in our laboratory to be adaptable to various organic bridging ligands (L). Extraction of the isolated crystals with warm anhydrous methanol can be used to remove any DMSO guests from the pores. Heating the extracted crystals under vacuum at 90–100 °C is sufficient to remove the methanol from the pores of the crystals and create a "guest-free" sorbent. For powder preparation, the single crystals were simply ground into powder, and packed into a thin capillary tubing for synchrotron data collection.

B. Synchrotron powder X-ray diffraction[1]

The powder pattern of Ni-BpyNH$_2$ was collected from a rotated 0.7 mm capillary specimen, using a wavelength of 0.412817 Å. High-resolution synchrotron X-ray powder diffraction data were collected using beamline 11-BM at the APS, Argonne National Laboratory. Discrete detectors covered a final angular range from 0° to 50°, with data points collected every 0.001° in 2θ at a scan speed of 0.01°/s. The instrumental optics of 11-BM incorporate two platinum-striped mirrors and a double-crystal Si (111) monochromator, where the second crystal has an adjustable sagittal bend (Wang et al., 2008). The diffractometer is controlled via EPICS (Dalesio et al., 1994). A vertical Huber 480 goniometer positions 12 perfect Si (111) analyzers and 12 Oxford-Danfysik LaCl$_3$ scintillators, with a spacing of 2° in 2θ (Lee et al., 2008). Capillary samples are mounted by a robotic arm and spun at ≈90 Hz. Data are normalized to incident flux and collected while continually scanning the diffractometer 2θ arm. A mixture of National Institute of Standard and Technology standard reference materials, Si (SRM™ 640e) (Walters, 2015) and Al$_2$O$_3$ (SRM™ 676) (Walters, 2008), was used to calibrate the instrument, where the Si lattice constant determines the wavelength for each detector. Corrections are applied for detector sensitivity, 2θ offset, and small detector wavelength differences, before merging the data into a single set of intensities evenly spaced in 2θ.

C. Rietveld refinements

Rietveld refinements were carried out using General Structure and Analysis System-II (Rietveld, 1969; Toby and Von Dreele, 2013). The initial model was from the previous single-crystal structure, removing the DMSO solvent. Only the 2.0°–30.0° portion of the pattern was included in the refinement ($d_{min} = 0.797$ Å). All non-H bond distances and angles were subjected to restraints, based on a Mercury/Mogul Geometry check (Sykes et al., 2011; Bruno et al., 2004). The Mogul average and standard deviation for each quantity were used as the restraint parameters. The Ni1–C2 bonds were restrained to 1.86(1) Å, the Ni2–N1 bonds to

[1] The purpose of identifying the equipment and software in this article is to specify the experimental procedure. Such identification does not imply recommendation or endorsement by the National Institute of Standards and Technology.

https://doi.org/10.1017/S0885715624000058 Published online by Cambridge University Press

2.07(1) Å, and the Ni2–N6 bonds to 2.11(1) Å. Planar restraints were also applied to the aromatic rings. The restraints contributed 2.5% to the final χ^2. The hydrogen atoms were included in calculated positions, which were recalculated during the refinement using Materials Studio (Dassault Systèmes, 2022). The U_{iso} of the heavy atoms was fixed. A fourth-order spherical harmonics model for the preferred orientation model was included; the refined texture index was 1.125. The peak profiles were described using the generalized microstrain model (Stephens, 1999). The background was modeled using a three-term shifted Chebyshev polynomial.

D. Powder X-ray pattern for inclusion in PDF

The deposited powder X-ray reference pattern was obtained using a Rietveld pattern decomposition technique (Toby and von Dreele, 2013). Using this technique, the reported peak intensities were derived from the extracted integrated intensities, and positions are calculated from the lattice parameters. When peaks are not resolved at the resolution function, the intensities are summed, and an intensity-weighted *d*-spacing is reported. The reported *d*-spacings are corrected for systematic errors via the inclusion of possible instrumental effects in the Rietveld fitting modal.

III. RESULTS AND DISCUSSION

Figure 1 gives the observed (crosses), calculated (solid line), and normalized difference X-ray diffraction (XRD) patterns (bottom) for Ni-BpyNH$_2$ using the Rietveld analysis technique. The vertical lines below the profiles mark the positions of all possible Bragg reflections. The final refinement of 44 variables using 28,045 observations and 33 restraints yielded the residuals $R = 0.088$, $R_{wp} = 0.2304$, and goodness of fit = 4.48. The largest errors in the difference plot (Figure 1) probably indicate the presence of un-model disordered extra-framework species, which were not apparent in a different Fourier map.

Since the bond distances and angles were restrained, all of them fall within normal ranges. The root-mean-square Cartesian displacement of the non-H atoms in the solvated single-crystal structure and the unsolvated powder structure

TABLE II. Atomic coordinates for Ni-BpyNH$_2$

Atom	*x*	*y*	*z*	Occ.	Site
Ni1	0	0.2519(4)	−0.0099(5)	1.0000	8f
Ni2	¼	0.1929(2)	¼	1.0000	8e
N1	−0.1586(9)	0.2915(9)	−0.1265(9)	1.0000	16g
N2	0.1497(12)	0.2030(8)	0.1256(14)	1.0000	16g
N3	¼	0.2875(4)	¼	1.0000	8e
N4	0.224(2)	0.4064(5)	0.0602(8)	0.2500	16g
H4A	0.16425	0.43009	0.04777	0.2500	16g
H4B	0.28278	0.40490	0.00167	0.2500	16g
N5	0.154(4)	0.4749(5)	0.406 (3)	0.2500	16g
H5A	0.14994	0.48979	0.48803	0.2500	16g
H5B	0.11355	0.43218	0.38260	0.2500	16g
N6	¼	0.5994(2)	¼	1.0000	8e
C1	−0.0875(9)	0.2740(9)	−0.1077(12)	1.0000	16g
C2	0.1021(11)	0.2260(9)	0.065(2)	1.0000	16g
C3	0.240(2)	0.3175(3)	0.1582(3)	1.0000	16g
H3	0.23356	0.29346	0.07819	1.0000	16g
C4	0.234(2)	0.3772(3)	0.1539(5)	1.0000	16g
C5	¼	0.4073(4)	¼	1.0000	8e
C6	¼	0.4726(4)	¼	1.0000	8e
C7	0.2033(10)	0.5038(3)	0.3268(9)	1.0000	16g
C8	0.2064(7)	0.5672(3)	0.3251(6)	1.0000	16g
H8	0.16896	0.58826	0.39376	1.0000	16g

(Space group: orthorhombic *Cmca*). The value of 0.01 was used as the U_{iso} value for the two Ni sites and 0.03 was used for the rest. Additional coordinates of H4 (0.2259, 0.4008,0.0780) as in C4–H4 and H7 (0.1646, 0.4811, 0.389) as in C7–H7 that are shown in Figure 2(b) are theoretical values each with an occupancy of 0.75, as a result of the disordered NH$_2$ groups. Values inside the brackets are one standard deviation.

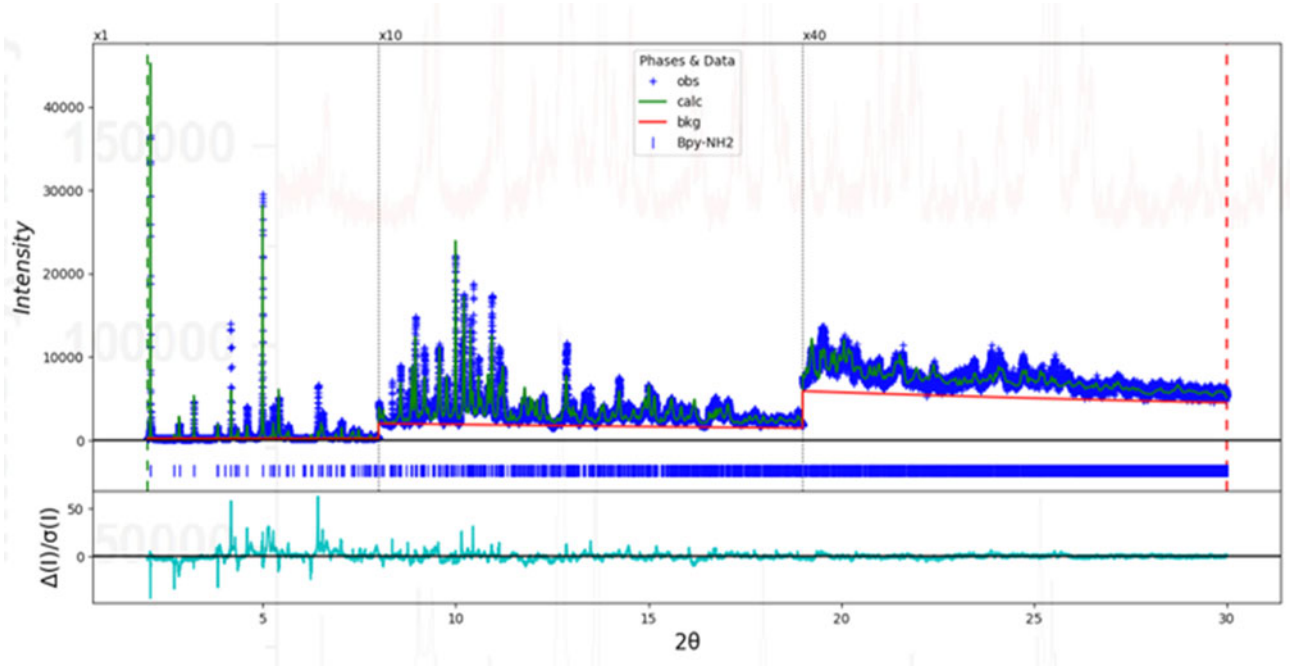

Figure 1. Observed (crosses), calculated (solid line), and normalized difference XRD patterns (bottom) for Ni-Bpy-NH$_2$ by the Rietveld analysis technique. The vertical lines below the profiles mark the positions of all possible Bragg reflections.

https://doi.org/10.1017/S0885715624000058 Published online by Cambridge University Press

TABLE III. Interatomic distances for Ni-BpyNH$_2$ and Ni-BpyNH$_2$(D)

		Distances (Å)	
Atom	Atom	Ni-BpyNH$_2$	Ni-BpyNH$_2$(D)
Ni1	C1	1.837(8)	1.860(4)
Ni1	C2	1.862(2)	1.861(4)
Ni2	N1	2.067(2)	2.067(3)
Ni2	N2	2.146(7)	2.048(3)
Ni2	N3	2.144(7)	2.135(4)
Ni2	N6	2.117 (4)	2.107(5)
N1	C1	1.143 (2)	1.165(4)
N2	C2	1.151(2)	1.150(5)
N3	C3	1.333(4)	1.332(5)
N4	C4	1.345(9)	1.48(2)
N5	C7	1.387(9)	1.36(2)
N6	C8	1.346(2)	1.336(5)
C3	C4	1.357(6)	1.394(6)
C4	C5	1.391(4)	1.387(7)
C5	C6	1.481(5)	1.483(9)
C6	C7	1.370(4)	1.404(6)
C7	C8	1.437(5)	1.382(6)

Values inside brackets are one standard deviation.

TABLE IV. Interatomic bond angles for Ni-BpyNH$_2$ and Ni-BpyNH$_2$(D)

			Angles (°)	
Atom	Atom	Atom	Ni-BpyNH$_2$	Ni-BpyNH$_2$(D)
C1	Ni1	C2	168.7(13)	177.7(2)
N2	Ni2	N2	167.7(11)	179.2(2)
N3	Ni2	N6	180.0	180.0
Ni1	C2	N2	164(2)	177.4(2)
Ni2	N2	C2	159(2)	174.3(2)
Ni2	N1	C1	143.7(11)	171.0(3)

Values inside brackets are standard deviations.

is 0.731 Å, indicating that the solvent has a significant effect on the framework.

The atomic coordinates and isotropic displacement factors including hydrogen atoms are shown in Table II. Table III lists the selected pertinent bond distances and Table IV gives the selected bond angles for Ni-BpyNH$_2$.

A. Powder X-ray pattern for inclusion in PDF

The X-ray powder diffraction pattern for Ni-BpyNH$_2$ has been submitted for inclusion in the PDF and will not be reported here. In the submitted pattern, the symbol "M" refers to peaks containing contributions from two overlapping reflections. The peak that has the strongest intensity in the entire pattern is assigned an intensity of 999 and other lines are scaled relative to this value. In general, the *d*-spacing values are calculated from refined lattice parameters. The intensity values reported are integrated intensities (rather than peak heights). For resolved overlapped peaks, intensity-weighted calculated d-spacing, along with the observed integrated intensity and the *hkl* indices of both peaks are used. For peaks that are not resolved at the instrumental resolution, the intensity-weighted average *d*-spacing and the summed integrated intensity value are used. In the case of a cluster, unconstrained profile fits often reveal the presence of multiple peaks, even when they are closer than the instrumental resolution. In this situation, both *d*-spacing and intensity values are reported independently.

B. Structure of Ni-BpyNH$_2$

The DMSO solvent of crystallization could not be located in the powdered Ni-BpyNH$_2$ as a result of the methanol extraction procedure. The structure of Ni-BpyNH$_2$ was found to be orthorhombic with a space group of *Cmca*, $a = 14.7218(3)$ Å, $b = 22.6615(3)$ Å, $c = 12.3833(3)$ Å, $V = 4131.29(9)$ Å^3, $Z = 8$, and $D_x = 1.253$ g-cm^{-3} (Table I). Figure 2(a) gives the basic

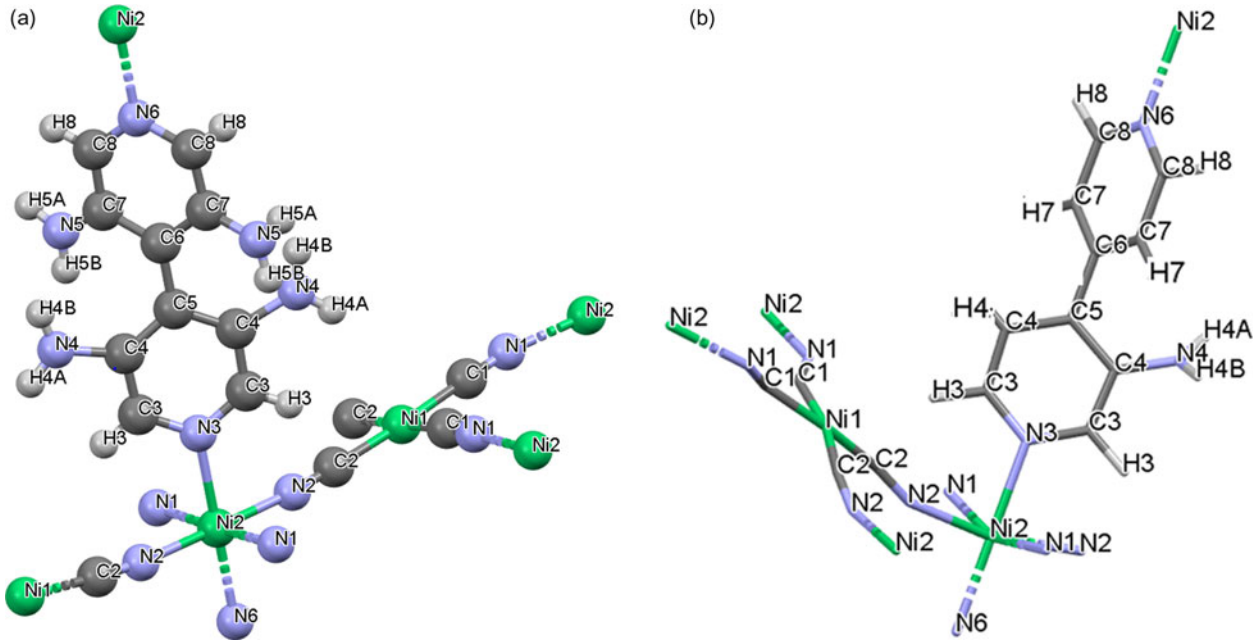

Figure 2. (a) Motif of Ni-BpyNH$_2$ (green – i, blue – N, gray – C) showing disordered NH$_2$ groups. H atoms are omitted for clarity. (b) A theoretical Ni-BpyNH$_2$ motif with ordered NH$_2$ group (green – Ni, blue – N, gray – C) showing one NH$_2$ group.

https://doi.org/10.1017/S0885715624000058 Published online by Cambridge University Press

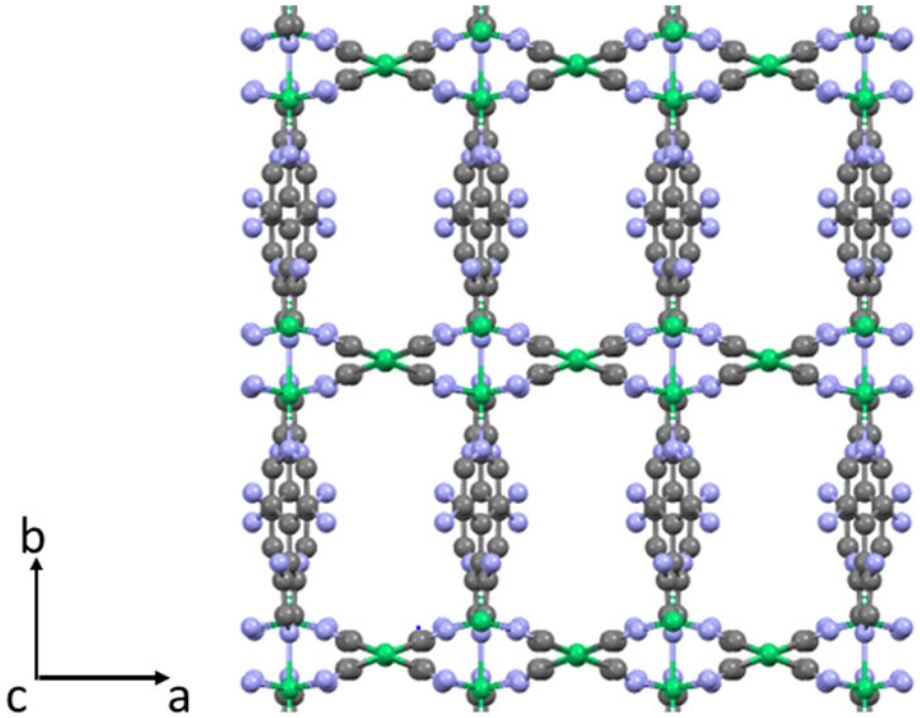

Figure 3. Packing diagram of Ni-BpyNH$_2$ viewing down the *c*-axis (green – Ni, blue – N, gray – C). H atoms are omitted for clarity.

motif of Ni(BpyNH$_2$)[Ni(CN)$_4$] with full atomic labels. In Figure 2(b), a theoretical Ni-BpyNH$_2$ motif with an ordered NH$_2$ group (green – Ni, blue – N, gray – C) showing one NH$_2$ group. Because of the absence of the solvent of crystallization, DMSO, the chemical formula of the compound is $Ni_2N_7C_{14}H_9$ as compared to $Ni_2N_7C_{18}S_2O_2H_{21}$.

Ni-BpyNH$_2$ forms a 3-D network, with a sinuous 2-D Ni(CN)$_4$ rectangular net connecting to each other via the BpyNH$_2$ ligands. The *b*-axis is much longer than that of *a*- and *c*- and that is where the long axis of the ligand BpyNH$_2$ aligns. Figure 3 gives the 3-D packing diagram of the structure, viewing along the *c*-axis. It is clear that the fundamental structure is similar to that of Ni-Bpene (Wong-Ng et al., 2013) and Ni-BpyMe (Wong-Ng et al., 2021b) where parallelepiped shape cavities were enclosed by the 2-D Ni(CN)$_4$ net and by the BpyNH$_2$ ligands. The 2-D Ni(CN)$_4$ net is connected to each other via the bonding of the pyridine N3 (and N6) atoms to Ni2. The Ni2 atom is of six-fold coordination to N with relatively long Ni2–N distances (average of 2.118 Å) (Table II) as compared to the much shorter four-fold coordination Ni1–C distances (average of 1.850 Å). Figure 4 gives the "projected view" of the net along the *a*-axis where

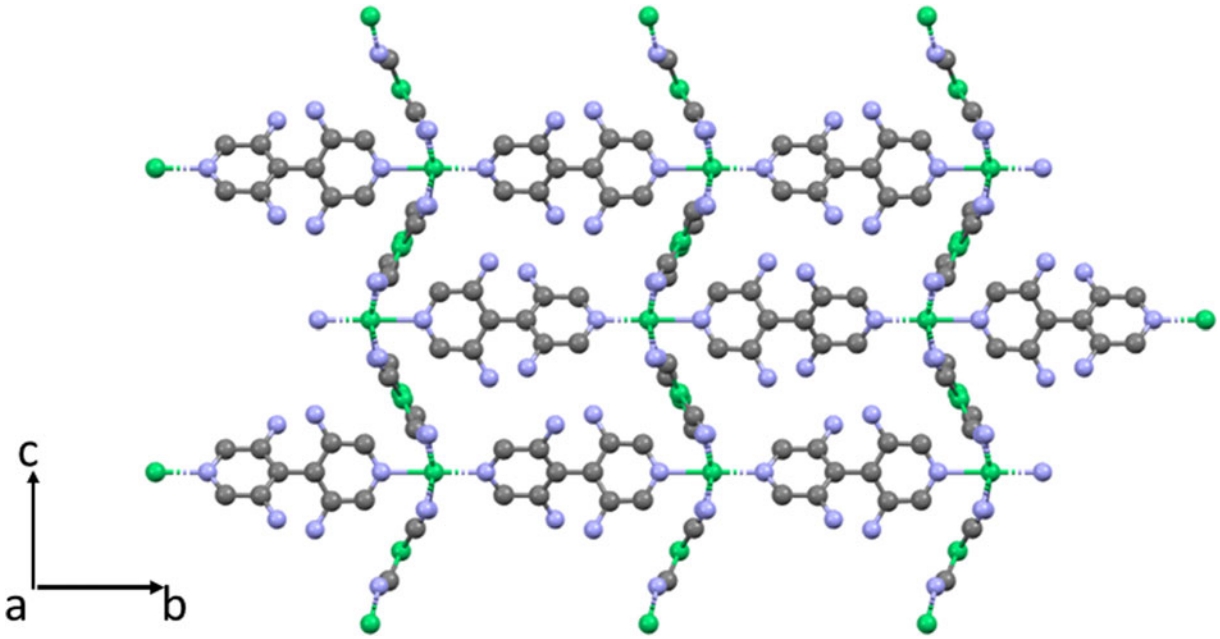

Figure 4. Packing diagram of Ni-BpyNH$_2$ viewing down the *a*-axis. (green – Ni, blue – N, gray – C). H atoms are omitted for clarity.

https://doi.org/10.1017/S0885715624000058 Published online by Cambridge University Press

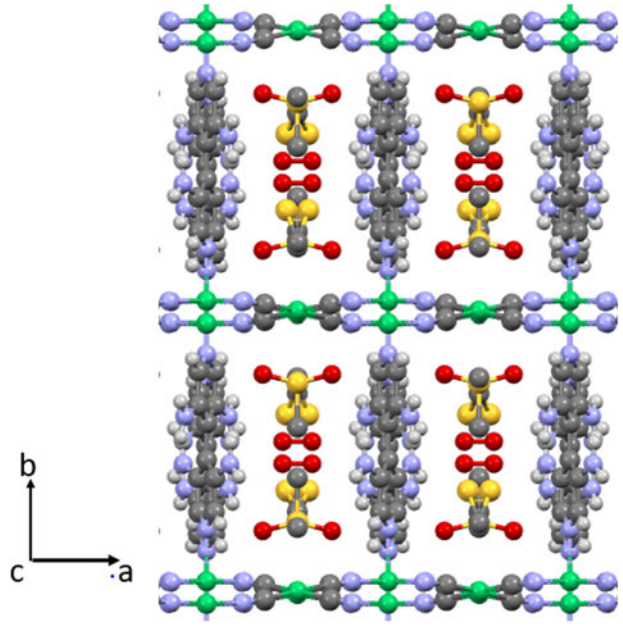

Figure 5. Packing diagram of Ni-BpyNH$_2$(D) viewing down the *c*-axis (Wong-Ng et al., 2016a) (green – Ni, blue – N, gray – C, yellow – S, and red – O). H atoms are omitted for clarity.

the NH_2 groups are pointing toward the center of the pores (hydrogen atoms are excluded for clarity). It is also clear that the pertinent bond angles around the 2-D net all deviated substantially from 180° (see Table III), giving rise to the sinuous appearance of the 2-D net.

The amine functional group, NH_2, was found in the *m*-position relative to the N atom of the pyridine ring and was disordered. Instead of having a unique "N" position, the resulting structure gives a total of four positions (two N4 and two N5) per ligand due to disorder, therefore each N4 and N5 only has a site occupancy of ¼ in each of the four *m*-positions. In other words, the NH_2 group has 25% probability of being at one of the four possible *m*-positions. Figure 2(b) gives the schematic of the ordered theoretical motif of Ni-BpyNH$_2$ where there is only one NH_2 group per ligand. The theoretical coordinates of H4 as in C4–H4 and H7 as in C7–H7 (Figure 2(b)) with an occupancy of 0.75 were computed to be (0.2259, 0.4008, 0.0780) and (0.1646, 0.4811, 0.389), respectively. The two pyridine rings in the ligands are not coplanar, they make an angle of approximately 40° to each other to avoid steric hindrance.

C. Comparison of the crystal structure of Ni-BPyNH$_2$ with Ni-BPyNH$_2$(D)

The lattice constants of solvent-free Ni-BPyNH$_2$ are smaller than that with solvent of crystallization, Ni-BPyNH$_2$(D), and were reported to be orthorhombic, space group *Cmca*. The unit cell dimensions of Ni-BPyNH$_2$(D) were determined to be $a = 14.7000(5)$ Å, $b = 22.6879(7)$ Å, $c = 13.8028(4)$ Å, $V = 4603.4(2)$ Å^3, and $Z = 8$ (Wong-Ng et al., 2016a) (Table I).

Tables III and IV give bond lengths and bond angles of both the solvated and unsolved compounds for comparison. In the solvated compound, apparently, the bond angles have a higher tendency to be linear than those in the unsolvated compound where they have more degrees of freedom for the movement of atoms, resulting in a structure with a more sinuous character (larger curvature of the net).

Figures 3 and 4 give the packing diagram of Ni-BpyNH$_2$ viewing down the *c*- and *a*-axis while Figures 5 and 6 give the packing for Ni-BPyNH$_2$(D) viewing along *c*- and *a*-axis, respectively. A comparison of the packing diagrams of Figure 3 with Figure 5, and Figure 4 with Figure 6 revealed

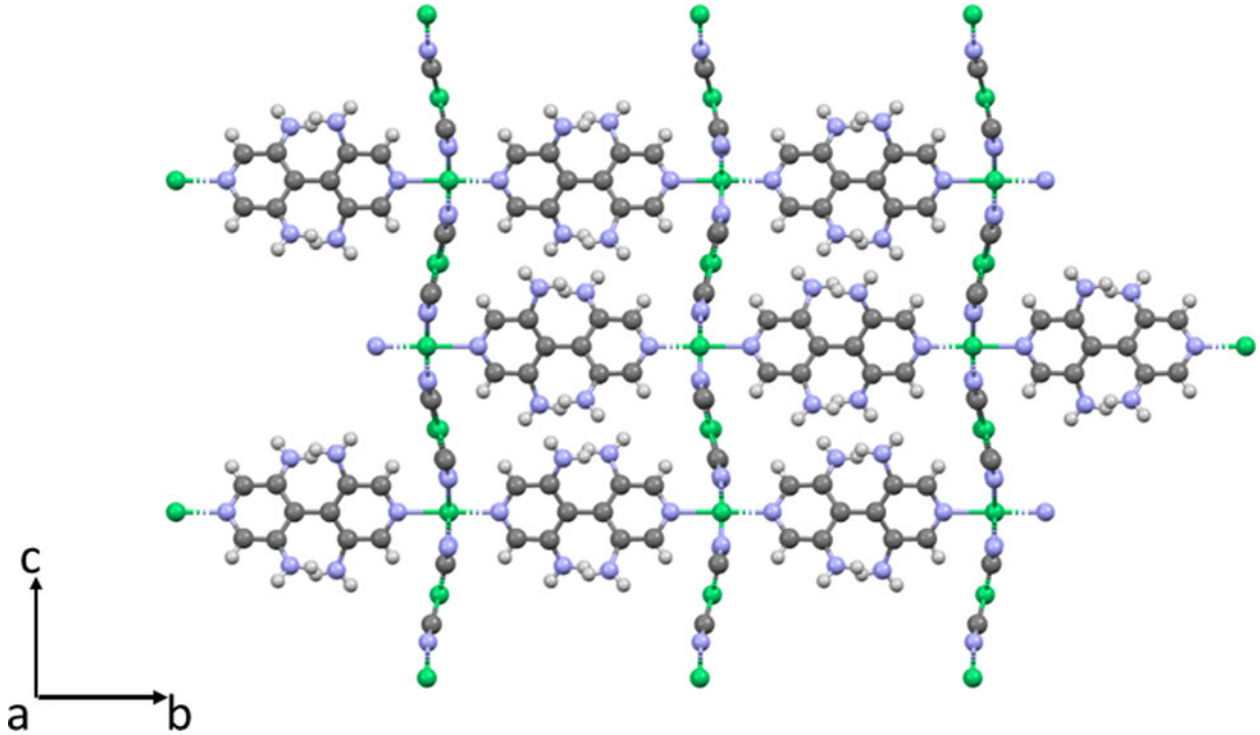

Figure 6. Packing diagram of Ni-BpyNH$_2$(D) viewing down the a-axis (Wong-Ng et al., 2016a) (green – Ni, blue – N, gray – C, yellow – S, and red – O).

https://doi.org/10.1017/S0885715624000058 Published online by Cambridge University Press

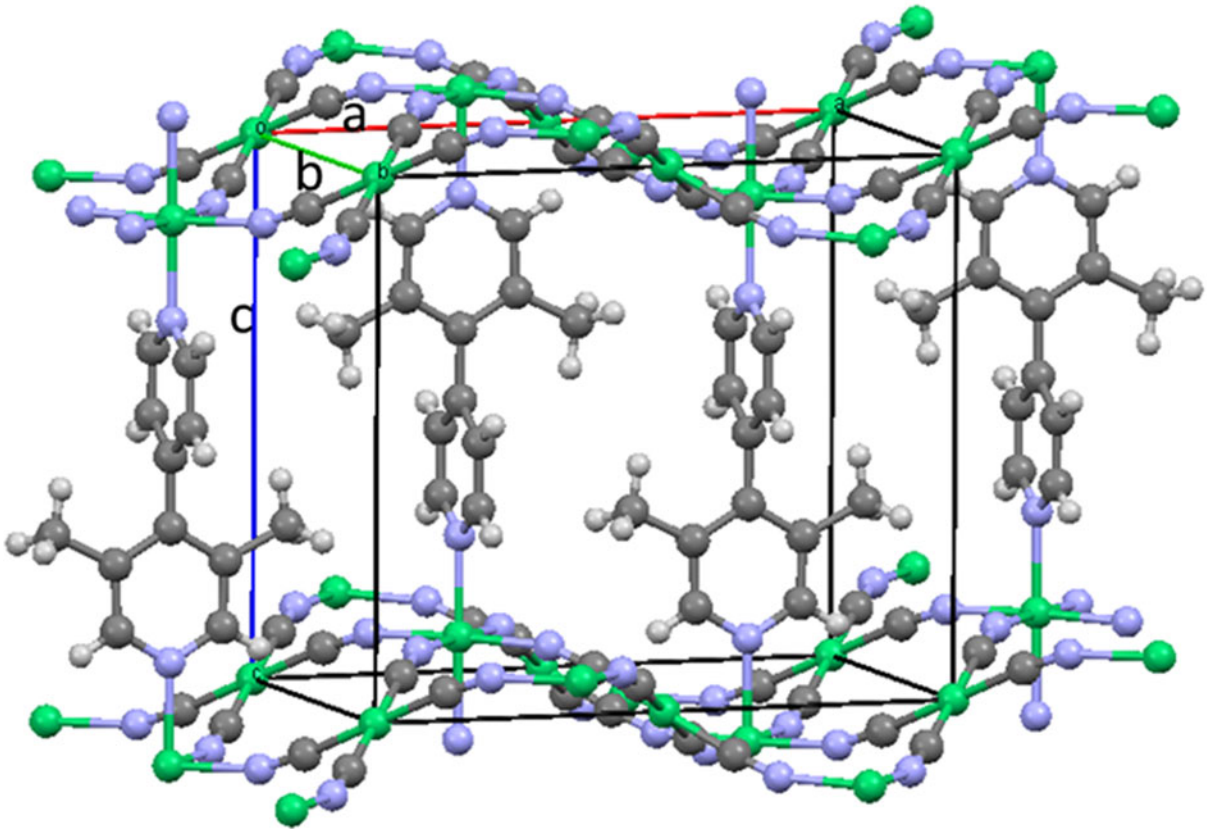

Figure 7. Packing diagram of Ni-BpyMe showing the curvature of the 2-D net and the orientations of the Bpy rings (Wong-Ng et al., 2021b) (green – Ni, blue – N, gray – C, off-white – H). Reprinted with permission from Elsevier Ltd.

that the 2-D net has a much lesser curvature in the structure with DMSO, probably because the solvent DMSO in the cavity prevented a high degree of curvature of the 2-D net. The average distances Ni2–N are somewhat longer in the guest-free structure than that in the DMSO-included sample (2.118 vs. 2.089 Å, respectively), whereas for the average Ni1–C bonds, the opposite situation was observed (1.850 Å in Ni-BPyNH$_2$ vs. the longer 1.860 Å in Ni-BPyNH$_2$(D)).

The dihedral angles formed between the two pyridine rings are larger in the solvent-free Ni-BPyNH$_2$ than that in Ni-BPyNH$_2$(D), (≈40° vs 25°, respectively). In another PICNIC structure, Ni-BpyMe (Wong-Ng et al., 2021b), where Me stands for the methyl group, it was reported that as a result of the large curvature of the 2-D net (Figure 7), the dispersive forces between the net and the ligands were maximized for achieving a stable structure. The similar situation is observed here in the structure of Ni-BPyNH$_2$.

IV. SUMMARY

The structure of guest-free Ni-BpyNH$_2$ has been determined and the reference powder pattern has been prepared and submitted to the PDF. The lattice parameters of the guest-free structure were found to be smaller than that with DMSO as a solvent of crystallization, as expected. The amine functional group, –NH$_2$, is disordered in both structures. The NH$_2$ group is found in the *m*-position relative to the N atom of the pyridine ring. Instead of having an unique position, it has ¼ site occupancy in each of the four *m*-positions. While the two structures are in general similar to each other, there are noticeable differences including a higher degree of curvature in the 2-D net of solvent-free Ni-BpyNH$_2$, presumably due to maximizing the dispersive forces between the ligands and the net (for stabilizing the structure). The dihedral angle between the two pyridine rings is greater in Ni-BpyNH$_2$ (≈40 °) than that in Ni-BpyNH$_2$(D) (≈25 °).

V. DEPOSITION DATA

The powder pattern of guest-free Ni-BpyNH$_2$ from the measured synchrotron data set has been submitted to ICDD for inclusion in the PDF. The Crystallographic Information Framework (CIF) file containing the results of the Rietveld refinement (including raw data) was deposited with the ICDD. The data can be requested from the PDJ managing editor at pdj@icdd.com."

ACKNOWLEDGEMENTS

The authors acknowledge ChemMatCARS Sector 15 which is principally supported by the National Science Foundation/Department of Energy under grant number NSF/CHE-1834750. Use of the Advanced Photon Source was supported by the U. S. Department of Energy, Office of Science, Office of Basic Energy Sciences, under Contract No. DE-AC0206CH11357. Partial financial support from the ICDD Grant-in-Aid Program #0903 is acknowledged.

CONFLICTS OF INTEREST

The authors declare none.

https://doi.org/10.1017/S0885715624000058 Published online by Cambridge University Press

REFERENCES

Allen, A. J., L. Espinal, W. Wong-Ng, W. L. Queen, C. M. Brown, S. R. Kline, J. T. Kauffman, J. T. Culp, and C. Matranga. 2015. "Flexible Metal-Organic Framework Compounds: *In Situ* Studies for Selective CO_2 Capture." *Journal of Alloys and Compounds* 647: 24–34. doi:10.1016/j.jallcom.2015.05.148.

Allen, A., W. Wong-Ng, E. Cockayne, L. A. Espinal, J. T. Culp, and C. Matranga. 2019. "Structural Basis of CO_2 Adsorption in a Flexible Metal Organic Framework Material." *Nanomaterials* 9 (3): 354–60. doi:10.3390/nano9030354.

Allen, A. J., E. Cockayne, W. Wong-Ng, J. T. Culp, and I. Kuzmenko. 2023. "Dynamic Structural and Microstructural Responses of a Metal Organic Framework Type Material to Carbon Dioxide Under Dual Gas Flow and Supercritical Conditions." *Journal of Applied Crystallography* 56: 222–36. doi:10.1107/S1600576722012134.

Brown, C. M., and J. R. Long. 2014. "Reversible CO Binding Enables Tunable CO/H_2 and CO/N_2 Separations in Metal-Organic Frameworks with Exposed Divalent Metal Cations." *Journal of American Chemical Society* 136 (30): 10752–61. doi:10.1021/ja505318p.

Bruno, I. J., J. C. Cole, M. Kessler, J. Luo, W. D. S. Motherwell, L. H. Purkis, B. R. Smith, R. Taylor, R. I. Cooper, S. E. Harris, and A. G. Orpen. 2004. "Retrieval of Crystallographically - Derived Molecular Geometry Information." *Journal of Chemical Information and Computer Sciences* 44: 2133–44. doi:10.1021/ci049780b.

Černák, J., and K. A. Abboud. 2000. "$Ni(bipy)_2Ni(CN)_4$, A New Type of One-Dimensional Square Tetracyano Complex." *Acta Crystallographica Section C* 56: 783–5. doi:10.1107/S0108270100004996.

Cockayne, E., W. Wong-Ng, Y. S. Chen, J. T. Culp, and A. J. Allen. 2021. "Density Functional Theory Study of the Structure of the Pillared Hofmann compound Ni(3-Methy- 4,4′-bipyridine)[$Ni(CN)_4$] (Ni-BpyMe or PICNIC 21)." *Journal of Physical Chemistry C* 125 (29): 15882–9. doi:10.1021/acs.jpcc.6b11692.

Culp, J. T., M. R. Smith, E. Bittner, and B. Bockrath. 2008a. "Hysteresis in the Physisorption of CO_2 and N_2 in a Flexible Pillard Layer Nickel Cyanide." *Journal of American Chemical Society* 130: 12427–34. doi:10.1021/ja802474b

Culp, J. T., S. Natesakhawat, M. R. Smith, E. Bittner, C. S. Matranga, and B. Bockrath. 2008b. "Hydrogen Storage Properties of Rigid Three-Dimensional Hofmann Clathrate Derivatives: The Effect of Pore Size." *Journal of Physical Chemistry C* 112: 7079–83. doi:10.1021/jp710996y.

Culp, J. T., C. Madden, K. Kauffman, F. Shi, and C. Matranga. 2013. "Screening Hofmann Compounds as CO_2 Srobents: Nontraditional Synthetic Route to over 40 Different Pore-Functionalized and Flexible Pillard Cyanonickelates." *Inorganic Chemistry* 52: 4205–16. doi:10.1021/ic301893p.

Dalesio, L. R., J. O. Hill, M. Kraimer, S. Lewis, D. Murray, S. Hunt, W. Watson, M. Clausen, and J. Dalesio. 1994. "Nuclear Instruments & Methods." *Physics Research Section A-Accelerators Spectrometers Detectors and Associated Equipment* 352: 179–84. doi:10.1016/0168-9002(94)91493-1.

Dassault Systèms. 2022. *Materials Studio 2023*. San Diego, CA, BIOVIA.

Espinal, L., D. L. Poster, W. Wong-Ng, A. J. Allen, and M. L. Green. 2009. "Standards, Data, and Metrology Needs for CO_2 Capture Materials – A Critical Review." *Environmental Science and Technology* 47: 11960–75. doi:10.1021/es402622q.

Espinal, L., W. Wong-Ng, J. A. Kaduk, J. Allen, C. R. Snyder, C. Chiu, D. W. Siderius, L. Li, E. Cockayne, A. E. Espinal, and S. L. Snyder. 2012. "Time Dependent CO_2 Sorption Hysteresis in a One-Dimensional Microporous Octahedral Molecular Sieve." *Journal of American Chemical Society* 134 (18): 7944–51. doi:10.1021/ja3014133.

Etheridge, D. M., L. P. Steele, R. L. Langenfelds, R. J. Francey, J. M. Barnola, and V. I. Morgan. 1996. "Natural and Anthropogenic Changes in Atmospheric CO_2 Over the Last 1000 Years from Air in Antarctic Ice and Fire." *Journal of Geophysical Research Atmospheric* 101 (D2): 4115–28. doi:10.1029/95JD03410.

Freund, R., O. Zaremba, G. Arnauts, R. Ameloot, G. Skorupskii, M. Dinca, A. Bavykina, J. Gascon, A. Ejsmont, J. Goscianska, M. Kalmutzki, U. Lächelt, E. Ploetz, S. Diercks, and S. Wuttke. 2021. "The Current Status of MOF and COF." *Angewandie Chemie International Edition* 60: 23975–24001. doi:10.1002/anie.202106259

Furukawa, H., K. E. O'Keeffe, and O. M. Yaghi. 2013. "The Chemistry and Applications of Metal-Organic Frameworks." *Science* 341: 1230444. doi:10.1126/science.1230444.

Gammon, R. H., E. T. Sundquist, and P. J. Fraser. 1985. History of carbon dioxide in the atmosphere in J. R. Trabalka (Ed.) *Atmospheric Carbon Dioxide and the Global Carbon Cycle*. DOE/ER-239, U.S. Department of Energy, Washington, D.C. pp. 25–62.

Gao, W.-Y., M. Chrzanowski, and S. Ma. 2014. "Metal-Metalloporphyrin Frameworks: Resurging Class of Functional Materials." *Chemical Society Review* 43: 5841–66. doi:10.1039/C4CS00001C.

Gates-Rector, S. D., and T. N. Blanton. 2019. "The Powder Diffraction File: A Quality Materials Characterization Database." *Powder Diffraction* 39: 352–60. doi:10.1017/S0885715619000812.

Hofmann, K. A., and F. Küspert. 1897. "Verbindungen von Kohlenwasserstoffen mit Metallsalzen." *Zeitschrift für anorganische und allgemeine Chemie* 15: 204–7. doi:10.1002/zaac.18970150118.

Kauffman, K. L., J. T. Culp, A. J. Allen, L. Espinal-Thielen, W. Wong-Ng, T. D. Brown, A. Goodman, M. P. Bernardo, R. J. Pancoast, D. Chirdon, and C. Matranga. 2011. "Selective Adsorption of CO2 from Light Gas Mixture by Using a Structurally Dynamic Porous Coordination Polymer." *Angewandie Chemie International Edition* 50: 10888–92. doi:10.1002/ange.201104130

Lawson, M., J. Horn, W. Wong-Ng, L. Espinal, S. H. Lapidus, H. G. Nguyen, Y. Meng, S. L. Suib, J. A. Kaduk, and L. Li. 2019. "Carbon Capture and Storage Properties of Porous Octahedral Molecular Sieve." *Powder Diffraction* 34 (1): 13–20. doi:10.1017/S0885715619000010.

Lee, P. L., D. Shu, M. Ramanathan, C. Preissner, J. Wang, M. A. Beno, R. B. Von Dreele, L. Ribaud, C. Kurtz, S. M. Antao, X. Jiao, and B. H. Toby. 2008. "A Twelve-Analyzer Detector System for High-Resolution Powder Diffraction." *Journal of Synchrotron Radiation* 15: 427–32. doi:10.1107/S090904950801843 84.

Liu, Y., Z. U. Wang, and H.-C. Zhou. 2012. "Recent Advances in Carbon Dioxide Capture with Metal-Organic Frameworks." *Greenhouse Gas Science Technology* 2: 239–59. doi:10.1002/ghg.1296.

Queen, W. L., M. R. Hudson, E. D. Bloch, J. A. Mason, M. I. Gonzalez, J. S. Lee, D. Gygi, J. D. Howe, K. Lee, T. A. Darwish, M. James, V. K. Peterson, S. J. Teat, B. Smit, J. B. Neaton, J. R. Long, and C. M. Brown. 2014. "Comprehensive Study of Carbon Dioxide Adsorption in the Metal-Organic Frameworks M_2(dobdc) (M = Mg, Mn, Fe, Co, Ni, Cu, Zn)." *Chemical Science* 5: 4569–81. doi:10.1039/C4SC02064B.

Rietveld, H. M. 1969. "A Profile Refinement Method for Nuclear and Magnetic Structures." *Journal of Applied Crystallography* 2: 65–71. doi:10.1107/S0021889869006558.

Stephens, P. W. 1999. "Phenomenological Model of Anisotropic Peak Broadening in Powder Diffraction." *Journal of Applied Crystallography* 32: 281–9. doi:10.1107/S0021889898006001.

Sykes, R. A., P. McCabe, F. H. Allen, G. M. Battle, I. J. Bruno, and P. A. Wood. 2011. "New Software for Statistical Analysis of Cambridge Structural Database Data." *Journal of Applied Crystallography* 44: 882–6. doi:10.1107/S0021889811014622.

Toby, B. H., and R. Von Dreele. 2013. "*GSAS-II*: The Genesis of a Modern Open-Source All Purpose Crystallography Software Package." *Journal of Applied Crystallography* 46 (2): 544–9. doi:10.1107/S0021889813003531.

Unnikrishnan, V., O. Zabihi, M. Ahmadi, Q. Li, P. Blanchard, A. Kiziltasb, and M. Naebe. 2021. "Metal–Organic Framework Structure–Property Relationships for High-Performance Multifunctional Polymer Nanocomposite Applications." *Journal of Materials Chemistry. A* 9: 4348–78. doi:10.1039/D0TA11255K.

Walters, R. L. 2008. NIST Standard References Materials 676a: Alumina Powder for Quantitative Analysis by X-ray Diffraction." Contact the NIST SRM program. e-mail address: srminfo@nist.gov

Walters, R. L. 2015. NIST Standard References Materials 640e: Line Position and Line Shape Standard for Powder Diffraction (Silicon Powder)." Contact the NIST SRM program. e-mail address: srminfo@nist.gov

Wang, J., B. H. Toby, P. L. Lee, L. Ribaud, S. Antao, C. Kurtz, M. Ramanathan, R. B. Von Dreele, and M. A. Beno. 2008. "A Dedicated Powder Diffraction Beamline at the Advanced Photon Source: Commissioning and Early Operational Results." *Review of Scientific Instruments* 79: 085105. doi:10.1063/1.2969260.

https://doi.org/10.1017/S0885715624000058 Published online by Cambridge University Press

Wong-Ng, W. 2018. "In Situ Diffraction Studies of Selected Metal-Organic Framework (MOF) Materials For Guest Capture/Exchange Applications". Chapter 4 "Materials and Processes for CO2 Capture, Conversion, and Sequestration." Wiley and Sons Publisher, ISBN 978-1-119-23103-5.

Wong-Ng, W., J. A. Kaduk, H. Wu, and M. Suchomel. 2012. "Synchrotron X-ray Studies of Metal-Organic Framework M_2(2,5-dihydroxytereph-thalte), M = (Mn,Co,Ni,Zn) (MOF74)." *Powder Diffraction* 27 (4): 256–62. doi:10.1017/S0885715612000863.

Wong-Ng, W., J. T. Culp, Y. S. Chen, P. Zavalij, L. Espinal, D. W. Siderius, A. J. Allen, S. Scheins, and C. Matranga. 2013. "Improved Synthesis and Crystal Structure of the Flexible Pillared Layer Porous Coordination Polymer: Ni(1,2-bis(4-pyridyl) ethylene)[Ni$(CN)_4$]." *Cryengcomm* 15: 4684–93. doi:10.1039/C3CE00017F.

Wong-Ng, W., J. A. Kaduk, D. L. Siderius, A. L. Allen, L. Espinal, B. M. Boyerinas, I. Levin, M. R. Suchomel, J. Ilavsky, L. Li, I. Williamson, E. Cockayne, and H. Wu. 2015. "Reference Diffraction Patterns, Microstructure, and Pore Size Distribution for the Copper (II) benzene-1,3,5-tricarboxylate Metal Organic Framework (Cu-BTC) Compounds." *Powder Diffraction* 30: 2–13. doi:10.1017/S0885715614001195.

Wong-Ng, W., J. T. Culp, Y. S. Chen, and C. Matranga. 2016a. "Crystallography of Representative Flexible MOFs Based on Pillard Cyanonickelate (PICNIC) Architecture." *CRYSTALS* 6 (9): 108. doi:10.3390/cryst6090108

Wong-Ng, W., J. T. Culp, Y.-S. Chen, J. Deschamps, and A. Marti. 2016b. "Flexible Metal Organic Framework {[Ni(DpBz)][Ni$(CN)_4$]}$_n$, DpBz = 1,4-Bis(4-pyridyl)benzene) with an Unusual Ni-N Bond." *Solid State Sciences* 52: 1–9. doi:10.1016/j.solidstatesciences.2015.11.010.

Wong-Ng, W., I. Williamson, M. Lawson, D. W. Siderus, J. T. Culp, Y. S. Chen, and L. Li. 2018. "Electronic Structure, Pore Size Distribution, and Sorption Characterization of an unusual MOF, {[Ni(dpbz)][Ni$(CN)_4$]}$_n$, dpbz = 1,4-bis(4-pyridyl)benzene." *Journal of Applied Physics* 123 (24): 245105. doi:10.1063/1.5031446.

Wong-Ng, W., G. T. McCandless, J. T. Culp, M. Lawson, Y. S. Chen, D. W. Siderius, and L. Li. 2021a. "Synchrotron Crystal Structure, Sorption Property and Electronic Structure of the Flexible MOF, Ni(Ni-4,4′azopyridine)[Ni$(CN)_4$]." *Solid State Sciences* 118: 106646. doi:10.1016/j.solidstatesciences.2021.106646.

Wong-Ng, W., J. T. Culp, D. W. Siderius, Y. S. Chen, S. Y. G. Wang, A. J. Allen, and E. Cockayne. 2021b. "Synthesis, Structural and Sorption Characterization of a Hofmann Compound, Ni(3-Methy- 4′- bipyridine)[Ni$(CN)_4$], for CO_2 Capture Application." *Polyhedron* 200: 115132. doi:10.1016/j.poly.2021.115132.

Zhou, H. C., and S. Kitagawa. 2014. "Metal–Organic Frameworks (MOFs)." *Chemical Society Review* 43: 5415–8. doi:10.1039/C4CS90059F

https://doi.org/10.1017/S0885715624000058 Published online by Cambridge University Press